Optically transparent circularly polarized THz dielectric resonator antenna for biomedical and industrial sub-THz applications

SAURABH KATIYAR[1,2,*], RAJVEER S. YADUVANSHI[3]
[1]*USICT, Guru Gobind Singh Indraprastha University, Delhi, India*
[2]*Amity University, Noida, India*
[3]*Netaji Subhas University of Technology, Delhi, India*

A novel circularly polarized optically transparent wideband dielectric resonator antenna (DRA) is presented in this work for THz band. The proposed DRA consists of a polyimide substrate incorporating a photonic band gap structure, with a transparent glass dielectric resonator (DR) placed on a slotted patch made of indium tin oxide. The proposed antenna achieves circular polarization and wide impedance bandwidth. Performance evaluation shows a peak gain of 6.5 dBi and a consistent LHCP radiation pattern. The proposed DRA is utilized for cancer detection. The shift in antenna's resonance frequency and reduction in gain of DRA help in detecting malign cells.

(Received July 11, 2024; accepted December 2, 2024)

Keywords: Transparent DRA, Circular polarization, THz band, Photonic band gap, Sensing and detection

1. Introduction

The International Telecommunication Union has designated the final portion of the electromagnetic spectrum as the terahertz (THz) frequency range (0.1 THz–3 THz) (ITU). THz radiation can be utilized to characterize materials since it easily passes through thin objects. This frequency band has special qualities like high-speed transmission over short distances and exceptional spatial resolution [1]. Compact antennas with positive gain are required for the applications indicated above. To do this, numerous antennas with high dielectric constant substrates and terahertz resonance have been constructed by various researchers. However, radiation efficiency degrades on such substrates. Terahertz radiation [2] can be produced with high radiation efficiency when the substrate is diced and there are defects in the usual patch shape. Micro-electromechanical systems are used to increase antenna gain, but the geometry grows complex and demands highly precise production [3]. The construction's complexity is reduced by using metamaterial structures [4] and layered geometry [5], but the antenna becomes bulky. Researchers also use the photonic crystal as an option to lessen the dielectric loss. The usage of PBG structures improves antenna properties [6] and 2D-fractal structures [8–10] with printed patch array and photonic crystal have been reported for THz applications. According to Zhang et al. [9,10], periodic PBG constructions with triangular, circular, and elliptical hollow air cylinders can be used to produce tuning frequency. Numerous variations in patch shapes [11,12], tapering geometry [13], and modifications in photonic crystal substrate material [14–17] have all been studied in-depth for THz applications. THz radiations are also a good substitute for X-rays, which are damaging when exposed to a body over an extended period due to their non-ionic nature [18–22]. There are various types of cancer, with breast cancer being the most prevalent among women [23]. While there are numerous cancer screening methods available, including EM radiation [24,25], magnetic resonance imaging [26], and spectroscopy [18], THz frequency cancer detection is a hotly debated research area [18,22,23,27-29]. Geetharamani [27,28] used rectangular and circular SRR-based antenna on ITO substrate. In [29] Khanjari et al. employed graphene substrate for THz frequency resonance and cancer detection.

The proposed Optically transparent THz DRA enables simultaneous optical transparency and THz functionality, which is useful for compact, multimodal systems. These antennas are critical for applications like security scanning, biomedical imaging, and high-speed THz communication. They can be integrated into transparent surfaces, such as smart windows or wearable devices, combining aesthetics with high performance. This technology supports next-gen networks and advanced sensing solutions.

In this work, we use ITO as a transparent sheet, which typically exhibits elevated sheet resistance in contrast to traditional conductive metals such as copper. Transparent conductive materials like ITO offer numerous benefits in THz antennas, despite their higher sheet resistance compared to metals like copper. These advantages encompass transparency, broader impedance bandwidth, flexibility, diminished electromagnetic interference (EMI), and enhanced adjustability [35-36]. The advantages of the presented work over existing designs are:

1. Optically Transparent Design: Utilizes ITO as a substrate, providing transparency and broadening potential application areas, especially where optical clarity is needed.
2. Compact and Efficient Structure: Achieves a compact footprint (450 × 450 μm²) with improved radiation efficiency, overcoming the limitations of high-dielectric constant substrates commonly used in THz antennas.
3. Circular Polarization and Wide Frequency Band: Operates with circular polarization and covers a broad frequency range (0.227 to 0.35 THz), ensuring robust performance and versatility across various THz applications.
4. Simplified Construction and Biomedical Potential: Reduces the complexity and bulk of traditional designs while offering promising applications in THz biomedical sensing, particularly for cancer detection.

Table 1. Comparison of proposed work with existing literature

Reference	Resonant Frequency (GHZ)	Impedance Bandwidth (GHz)	Gain (dBi)	Polarization	3- dB ARBW (GHz)	Dimensions (mm^2)
Proposed	**260**	**249-350**	**6.5**	**CP**	**255-350**	**0.45 × 0.45**
[35]	750	719-791	3.35	LP	-	0.88 × 0.76
[38]	0.15	0.03–0.1 THz	7	LP	-	15×20
[37]	6.5	6.4-7	5	LP	-	50×50

2. Design and analysis of optically transparent DRA

Fig. 1 presents the proposed circularly polarized DRA. A transparent polyimide substrate with a thickness of 15 μm with 3.5 relative permittivity (electrical conductivity = 0.0027) is used in DRA design on which the top surface consists of a corner truncated patch with an asymmetrical slot in the center of the patch. Optically transparent indium tin oxide (ITO) is utilized to construct the slotted patch fed by a microstrip line along with the ground plane of the polyimide substrate, which is designed using the conductive film of ITO. The 400 nm thick ITO thin film is used for designing with optical transmittance greater than 80% and electrical conductivities of 2.88× 105 S/m [35-36]. Drilling periodic air cross-shaped holes into a polyimide substrate (relative dielectric constant, ϵr = 3.5) results in the PBG-based polyimide configuration. Each hole is drilled at a distance of 75 μm with depth of 15 μm. A dielectric resonator of $MgAl_2O_4$ transparent ceramic is placed over the slotted ITO patch to excitation DRA. The DRA is developed for slot excitation with the fundamental HE11δ modes in consideration. High-purity MgO and γ-Al_2O_3 powders are used to create the transparent microwave dielectric ceramic by combining aqueous gel-casting with cold isostatic pressing, pressure-less sintering, and hot isostatic pressing techniques. [37]. Optimum relative permittivity ~8.2. The patch's width is calculated using,

$$W_p = \frac{2M+1}{\sqrt{\epsilon_r}} \times \frac{\lambda_0}{2}$$

where M is a non-negative number that, in this instance, is taken to be zero and λ_0 is the wavelength of free space. The dimensions of the slotted ITO patch and air-filled cross-shaped holes are shown in Fig. 2. While the modification in the patch's design significantly enhances its performance near 200 GHz, the slots sliced through the patch allow surface waves to flow through and boost antenna radiation performance.

The patch antenna with a slot can be modeled as a resonant cavity. The resonant frequencies and field distributions of the modes within the cavity can be determined by solving Maxwell's equations with appropriate boundary conditions. The electric field within the cavity can be expressed as a superposition of the modes:

$$E(x, y, z) = \Sigma [A\_mn * \Psi\_mn(x, y, z)] \quad (1)$$

where: A_mn are the complex amplitudes of the modes and Ψ_mn(x, y, z) are the mode functions representing the spatial distribution of the electric field for each mode (m, n)

The dielectric resonator placed on or near the patch modifies the effective permittivity seen by the cavity. This shifts the resonant frequencies of the modes. The perturbation in the resonant frequency due to the dielectric resonator can be approximated as:

$$\Delta f\_mn / f\_mn = - (1/2) * \iiint [\Delta\varepsilon\_r(x, y, z) * |\Psi\_mn(x, y, z)|^2] dV / \iiint [\varepsilon\_r(x, y, z) * |\Psi\_mn(x, y, z)|^2] dV \quad (2)$$

where: Δf_mn is the change in resonant frequency of mode (m, n), f_mn is the original resonant frequency of mode (m, n), Δε_r(x, y, z) is the change in relative permittivity due to the resonator, ε_r(x, y, z) is the original relative permittivity distribution. The integrals are taken over the volume of the cavity.

To achieve circular polarization, two orthogonal modes need to be excited with equal amplitudes and a 90° phase difference. Mathematically, if Ex and Ey are the

complex amplitudes of the orthogonal components of the radiated electric field, then for circular polarization:

$$|Ex| = |Ey| \quad (3)$$

and

$$\arg(Ex) - \arg(Ey) = \pm 90° \quad (4)$$

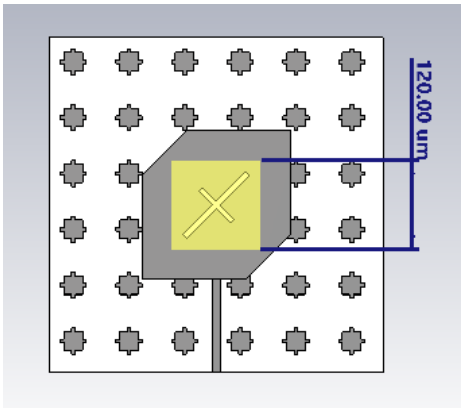

(a)

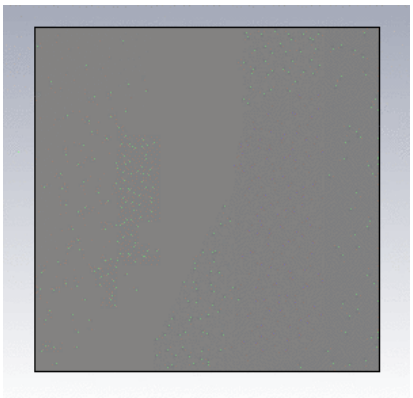

(b)

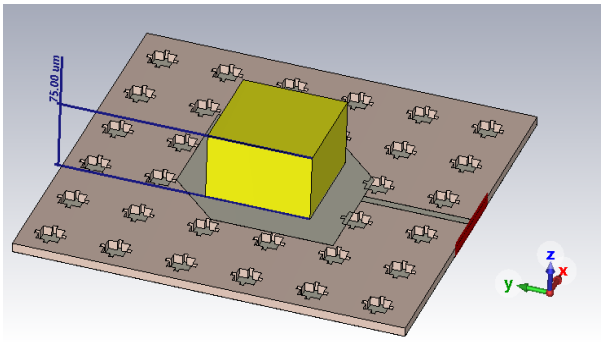

(c)

Fig. 1. Configuration of polyimide-based transparent DRA (a) top view (b) bottom view (c) side view (color online)

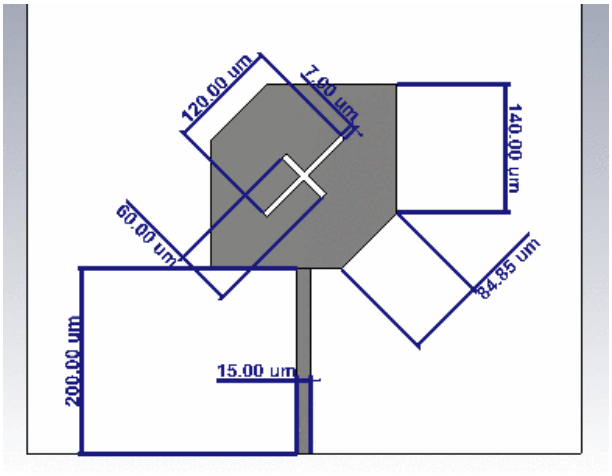

(a)

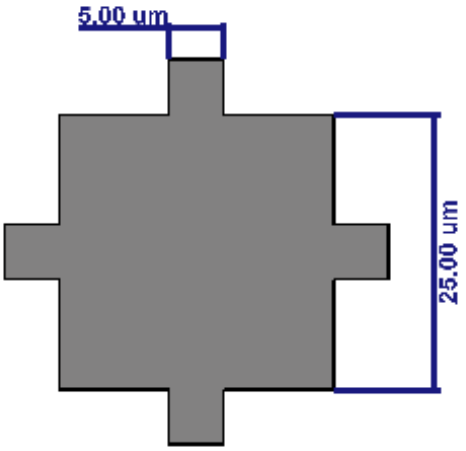

(b)

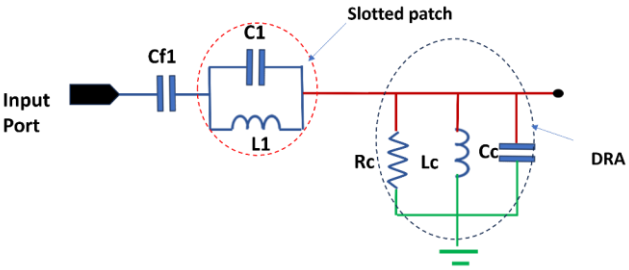

Fig. 2. (a) Dimensions of the patch and feed (b) dimensions of the cross-shaped hole in substrate (c) ECM of proposed DRA (color online)

The proposed DRA equivalent circuit diagram is developed using the circuit theory technique. The proposed DRA's equivalent circuit model (ECM) is shown in Fig. 2(c). The ECM consists of DRA which is demonstrated by parallel RLC model resonating in wideband and slots in the patch antenna are shown by parallel LC model and Cf is used to show the feeding capacitance.

3. Comparison analysis of polyimide substrate with and without PBG stuctures

The reflection properties of prototype antennas with homogeneous substrates and those with PBG-based polyimide substrates are compared in Fig. 3(a) in order to determine the edge of the PBG-based polyimide substrate over the homogeneous polyimide substrate. It is observed that the impedance bandwidth of the patch antenna with homogenous substrate is 0.242 to 0.278 THz while with PBG based polyimide substrate the impedance bandwidth of the antenna 0.246 to 0.281 THz. The impedance bandwidth of the patch antenna with PBG slightly shifts towards right side due to the inclusion of air holes in the substrate which in turn effect the permittivity of the substrate. The axial ratio value of the proposed antenna are shown in Fig. 3(b), the proposed antenna in case of both the substrates exhibits the complete overlapping of impedance bandwidth and 3-dB ARBW. The gain values of the antenna with and without PBG substrate are shown in Fig. 3(c) and it is observed that due to the inclusion of air-filled holes in the substrate the peak gain of the antenna is improved by 1.2 dB. Additionally, Fig. 3(c) implies that an antenna with a PBG substrate always has a higher gain than its equivalent. As can be shown, the antenna with the polyimide substrate based on PBG performs better than the antenna with a homogenous substrate. This is because the photonic structure suppresses surface waves, which makes using this substrate appropriate. When the radiation properties of the proposed antenna are compared to those of the current ones, we discover that the polyimide substrate with homogeneous ground that is based on PBG performs better in terms of matching the feedline better and having a lower reflection coefficient value. The simulated normalized radiation patterns of the proposed antenna with homogeneous and PBG polyimide substrate are shown in Fig. 4 at 0.275 THz. Proposed antenna is LHCP nature for both the substrates with RHCP below 15 dB. However, the radiation pattern of the DRA with PBG is more directive, which leads to higher gain.

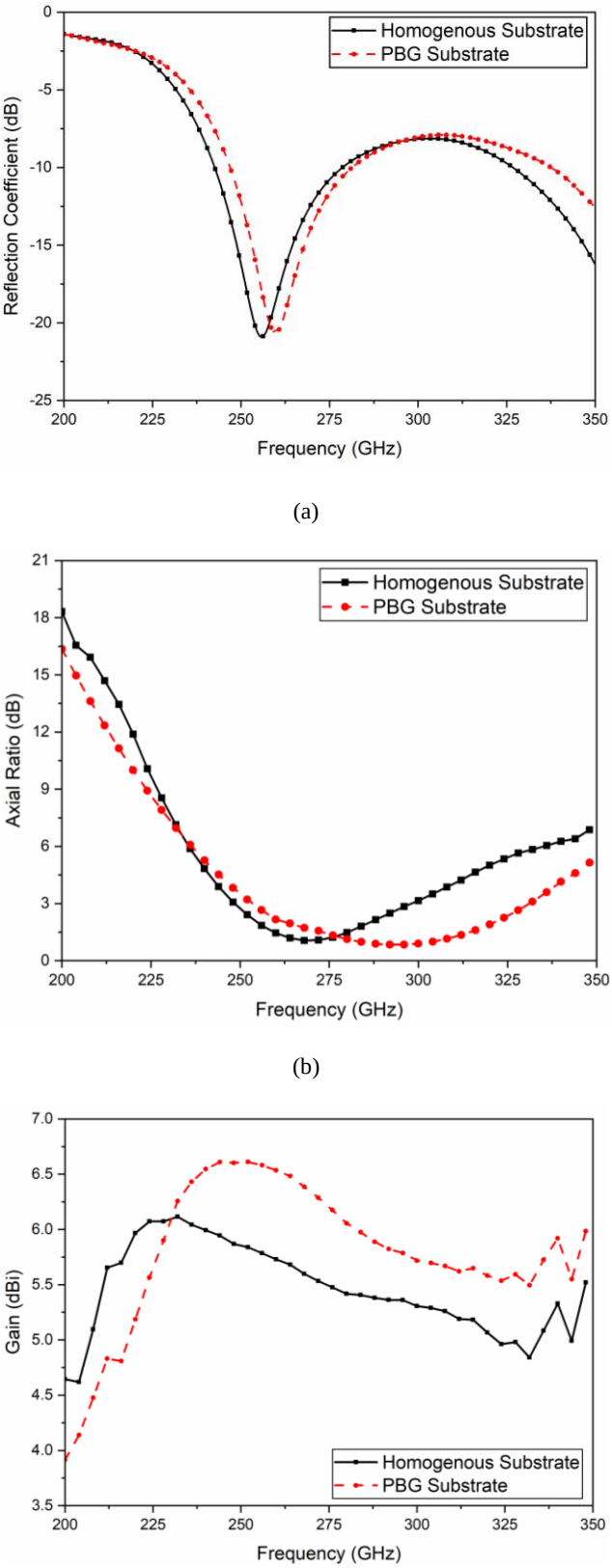

Fig. 3. Comparison of (a) reflection coefficient (b) axial ratio (c) gain values of the antenna with and without polyimide substrate (color online)

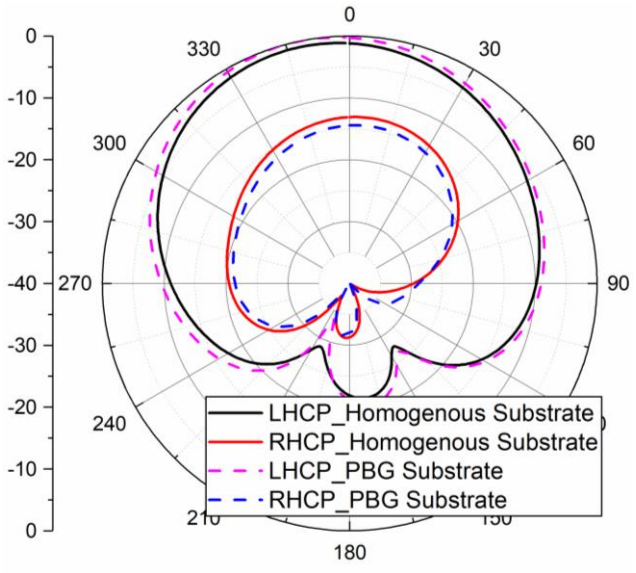

(a)

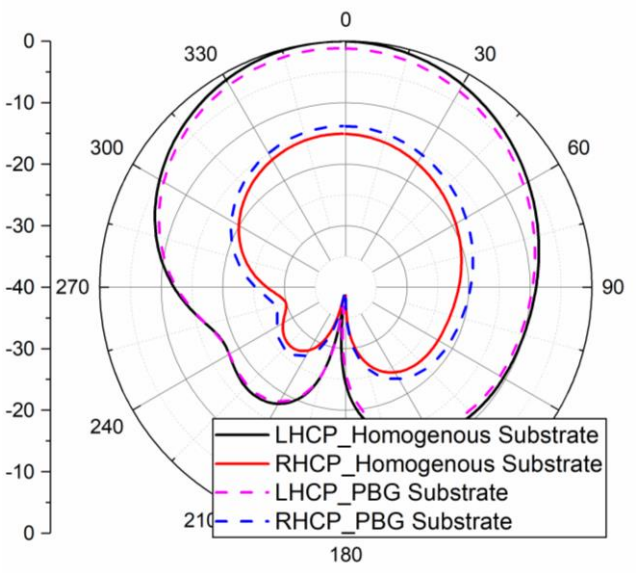

(b)

Fig. 4. Normalized radiation pattern of the antenna with and without PBG structure at 275 GHz (a) Phi=0-degree (b) Phi=90 degree (color online)

From Fig. 5(a), it can be observed that in the case of a simple patch DRA, the impedance matching is low, with an impedance bandwidth of 0.25 to 0.275 THz. Introducing truncation in the patch slightly improves the impedance bandwidth. Additionally, with the introduction of an asymmetrical cross-slot in the patch, a new resonance is observed, and the impedance bandwidth extends to 0.25 to 0.35 THz.

The axial ratio comparison for all three DRA configurations is presented in Fig. 5(b). In the case of the simple patch DRA, the antenna is not circularly polarized but exhibits elliptical polarization due to the PBG substrate. By introducing diagonal truncation in the patch, orthogonal fields are excited, allowing the DRA to achieve circular polarization (CP) in the 0.335 to 0.350 THz band. Furthermore, with the addition of the asymmetrical cross-slot, the 3-dB axial ratio bandwidth (ARBW) is enhanced to cover the 0.260 to 0.325 THz range.

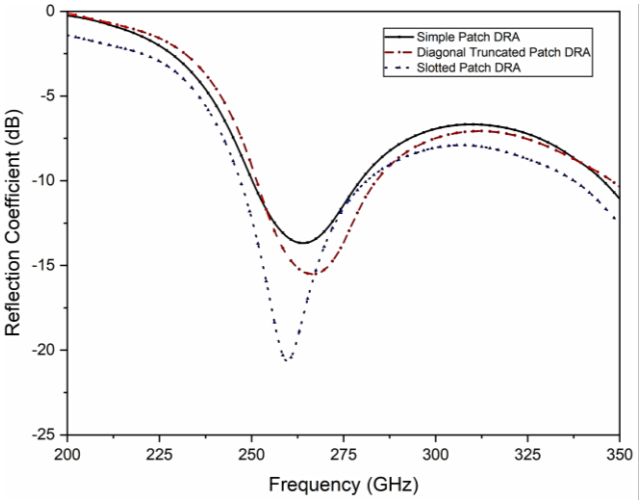

(a)

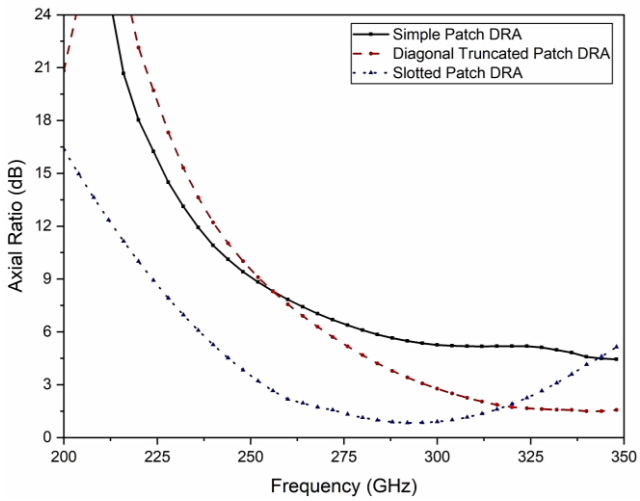

(b)

Fig. 5. Evolution of proposed DRA (a) reflection coefficients (b) axial ratio (color online)

4. Application of proposed DRA for breast cancer detection

As shown in Fig. 6, the three-dimensional healthy breast model is composed of layers of fibrous tissue and natural fat. With a 900 x 900 × 220 μm³ sizing, the model minimizes computing time [28]. Between the fibrous and normal fat layers in an infected breast, there is also a tumour layer, seen in black in Fig. 6(b). In the THz frequency range, normal fat, fibrous tissue, and tumours have relative permittivity values of 2.41, 2.80, and 3.18, respectively [23], [39]. The normal and diseased breast models serve as superstrates for the prototype antenna that

was described in the preceding sections. The standard refers to the obtained radiation parameters of the antenna using normal breast tissue as the superstrate, which is then compared to those of the antenna with the infected breast superstrate. As seen from Fig. 7(a), as the tumor is introduced in the phantom model the resonant frequency of the antenna shifts towards the lower frequency region. The resonant frequency of antenna, antenna with normal phantom, and antenna with tumor phantom is 263, 247, and 217 GHz, respectively. It is clear that the existence of a tumor causes the antenna's resonant band to shift, pointing to a deviation in the breast's inherent dielectric characteristics and raising the possibility of a tumor. Furthermore, it is evident from Fig. 7(b) that the presence of a tumor alters the gain values from the standard when they are compared to those of the infected breast superstrate. The antenna gain of the proposed DRA is reduced in the tumor phantom due to the change in dielectric value. As the dielectric value of the phantom is increased as compared to air, it causes more dielectric losses which lead to a reduction in gain values. Fig. 8 shows the normalized radiation pattern of the antenna at 215 GHz for the tumor phantom antenna. It shows that, in the boresight direction, the RHCP pattern is below the 15 dB LHCP pattern. Therefore, the prototype antenna is a good choice since it allows us to identify cancer by analyzing variations in the radiation characteristics of the antenna.

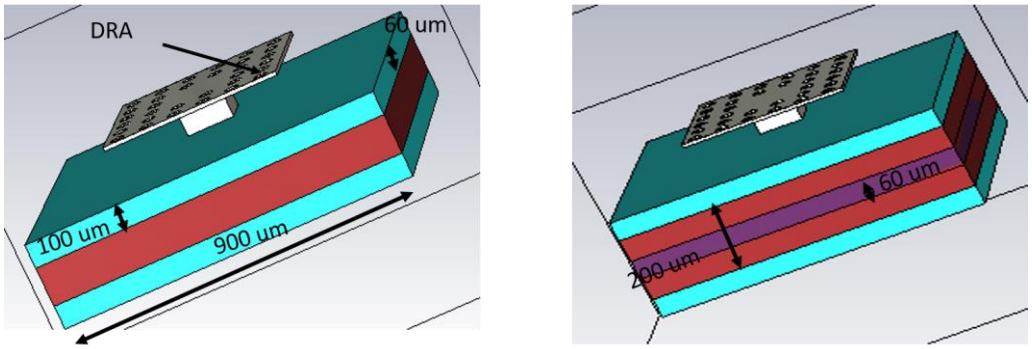

(a) (b)

Fig. 6. Proposed antenna integrated with breast phantom (a) without tumor (b) with tumor (color online)

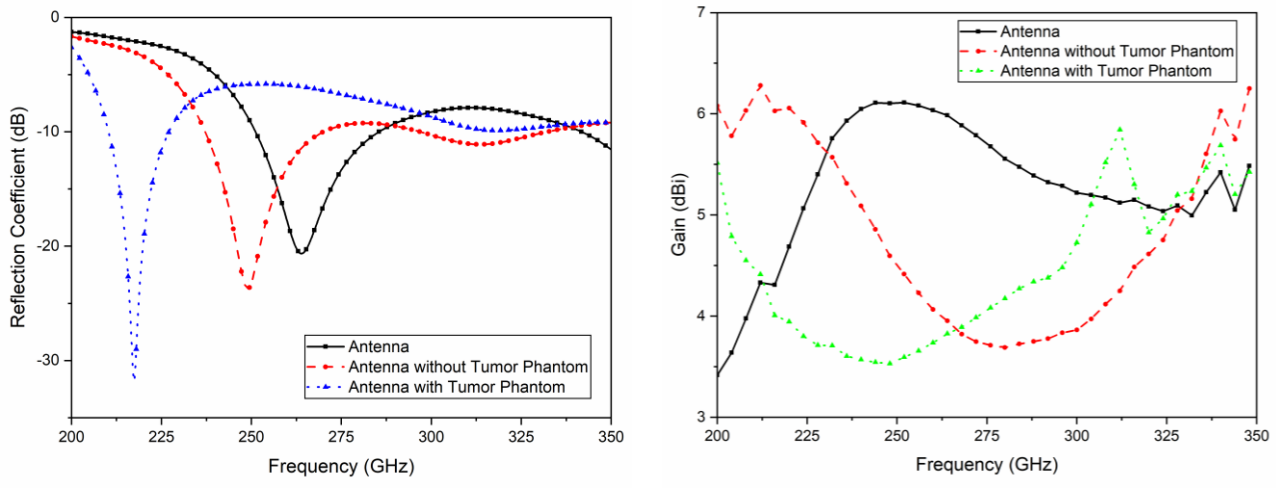

(a) (b)

Fig. 7. Comparison of (a) reflection coefficient (b) gain of proposed antenna with and without tumor (color online)

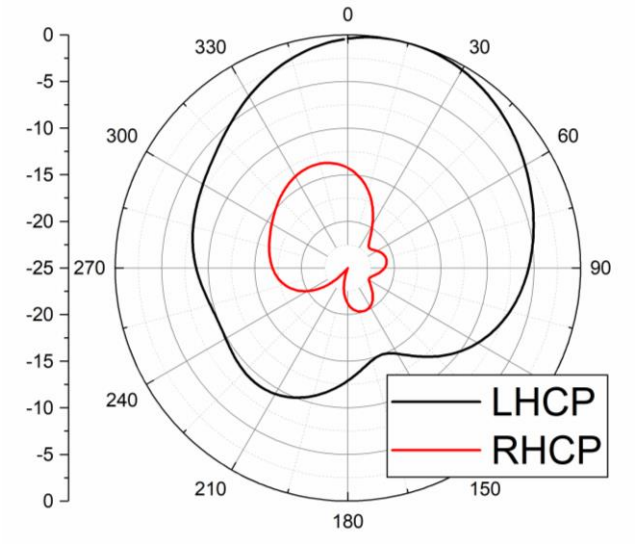

(a)

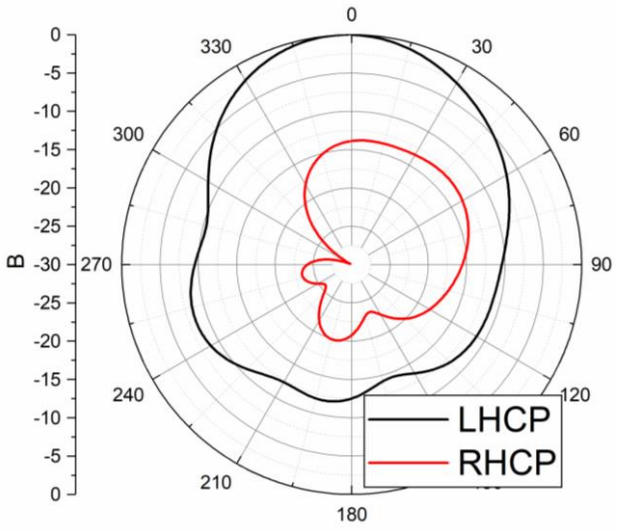

(b)

Fig. 8. Normalized radiation pattern of proposed antenna with tumor phantom (a) Phi=0 degree (b) Phi=90 degree (color online)

5. Conclusion

This paper presents a novel optically transparent CP wideband DRA for the THz band. The antenna achieves circular polarization with a 3-dB ARBW from 0.25 to 0.325 THz and impedance bandwidth from 0.227 to 0.35 THz by using indium tin oxide (ITO) as a transparent conducting material. A peak gain of 6.5 dBi and a steady left-hand circularly polarized radiation pattern demonstrates the antenna's performance. Furthermore, the notable resonance frequency shift and gain drop in the presence of a malignant model illustrate the antenna's efficacy in cancer detection. This highlights the potential of the suggested DRA for a range of THz applications, especially in imaging and medical diagnostics.

References

[1] S. Koenig, D. Lopez-Diaz, J. Antes, F. Boes, R. Henneberger, A. Leuther, A. Tessmann, R. Schmogrow, D. Hillerkuss, R. Palmer, T. Zwick, Nature Photonics **7**(12), 977 (2013).
[2] K. H. Alharbi, A. Khalid, A. Ofiare, J. Wang, E. Wasige, IET Microw. Antennas Propag. **11**(3), 310 (2016).
[3] L. Guo, F. Huang, X. Tang, Optik **125**, 101 (2014).
[4] Y. D. Sirmaci, C. K. Akin, C. Sabah, Opt. Quantum Electron. **48**(2), 1 (2016).
[5] K. Mak, K. So, H. Lai, K. Luk, IEEE Trans. Antennas and Propagation **65**(12), 6395 (2017).
[6] N. Singh, S. Singh, R. K. Sarin, 2010 10th Mediterranean Microwave Symposium, pp. 81–85 (2010).
[7] K. R. Jha, G. Singh, Infrared Phys. Technol. **55**(1), 32 (2012).
[8] H.-F. Zhang, AIP Adv. **7**(7), 075102 (2017).
[9] Z. Feng, Y.-Q. Chen, Phys. Plasmas **24**, 042116 (2017).
[10] H.-F. Zhang, S.-B. Liu, AIP Adv. **6**(8), 085116 (2016).
[11] A. Nejati, R. A. Sadeghzadeh, F. Geran, Physica B **449**, 113 (2014).
[12] A. Singh, S. Singh, Photon. Nanostruct.: Fundam. Appl. **14**, 52 (2015).
[13] U. Keshwala, S. Rawat, K. Ray, Optik **223**, 165648 (2020).
[14] A. S. Dhillon, D. Mittal, E. Sidhu, Optik **144**, 634 (2017).
[15] A. Sreekantan Thampy, D. Kumar, R.-J. Wu, M. Chavali, Optik **125**, 5546 (2014).
[16] R. K. Kushwaha, P. Karuppanan, L. Malviya, Physica B **545**, 107 (2018).
[17] M. S. Rabbani, H. Ghafouri-Shiraz, Microw. Opt. Technol. Lett. **57**(11), 2585 (2015).
[18] A. Alibadi, Q. Cassar, T. Zimmer, G. MacGrogan, L. Mavarani, P. Hillger, J. Grzyb, U. Pfeiffer, J.-P. Guillet, P. Mounaix, Biomedical Optics Express **9**, 1 (2017).
[19] T. Bowman, M. El-Shenawee, L. K. Campbell, IEEE Trans. Antennas and Propagation **63**(5), 2088 (2015).
[20] B. Truong, T. Hoang, A. Fitzgerald, V. Wallace, H. Nguyen, IEEE Trans. Bio-Med. Eng. **62**, 699 (2015).
[21] B. Peter, S. Yngvesson, P. Siqueira, P. Kelly, A. Khan, S. Glick, A. Karellas, IEEE Trans. Terahertz Sci. Technol. **3**, 374 (2013).
[22] I. Malhotra, K. R. Jha, G. Singh, Int. J. Microw. Wirel. Technol. **10**(3), 271 (2018).
[23] M. V. Hidayat, C. Apriono, AIP Conf. Proc. **2092**(1), 020020 (2019).
[24] S. Rahmatinia, B. Fahimi, IEEE Trans. Magn. **53**(6), 1 (2017).
[25] J. Bourqui, M. Kuhlmann, D. Kurrant, B. Lavoie, E. Fear, Sensors **18**, 1340 (2018).
[26] R. Balaji, K. Ramachandran, Breast Care **4**(3), 189 (2009).

[27] G. Geetharamani, T. Aathmanesan, SN Appl. Sci. **1**, article number 595 (2019).
[28] G. Geetharamani, T. Aathmanesan, Opt. Laser Technol. **126**, 106111 (2020).
[29] S. Poorgholam-Khanjari, F. B. Zarrabi, Opt. Commun. **480**, 126482 (2021).
[30] A. Anisha, D. Sriram Kumar, Optik **260**, 168959 (2022).
[31] A. R. Chishti, A. Aziz, M. A. Qureshi, M. N. Abbasi, A. M. Algarni, A. Zarguine, N. Hussain, R. Hussain, Appl. Sci. **13**(1), 210 (2022).
[32] A. Desai, C. D. Bui, J. Patel, T. Upadhyaya, G. Byun, T. K. Nguyen, IEEE Access **8**, 194206 (2020).
[33] A. Desai, M. Palandoken, J. Kulkarni, G. Byun, T. K. Nguyen, IEEE Access **9**, 147003 (2021).
[34] A. Desai, M. Palandoken, I. Elfergani, I. Akdag, C. Zebiri, J. Bastos, J. Rodriguez, R. A. Alhameed, Electronics **11**(2), 251 (2022).
[35] Anand Sreekantan Thampy, Sriram Kumar Dhamodharan, E: Low-dimensional Systems and Nanostructures **66**, 52 (2015).
[36] Ankit Sharma, Deepak Gangwar, Madan Kumar Sharma, Optical and Quantum Electronics **55**, 1282 (2023).
[37] Du, Chao, H. H. Guo, D. Zhou, H. T. Chen, J. Zhang, W. F. Liu, J. Z. Su, H. W. Liu, Journal of Materials Chemistry C **8**, 14880 (2020).
[38] Madan Kumar Sharma, Optical and Quantum Electronics **55**(9), 821 (2023).
[39] Madan Kumar Sharma, Satya P. Singh, Paarth Badola, Mithilesh Kumar, J. P. Saini, Aime' Lay Ekuakille, IEEE Sensors Journal **23**, 20207 (2023).

*Corresponding author: saurabh0277@gmail.com